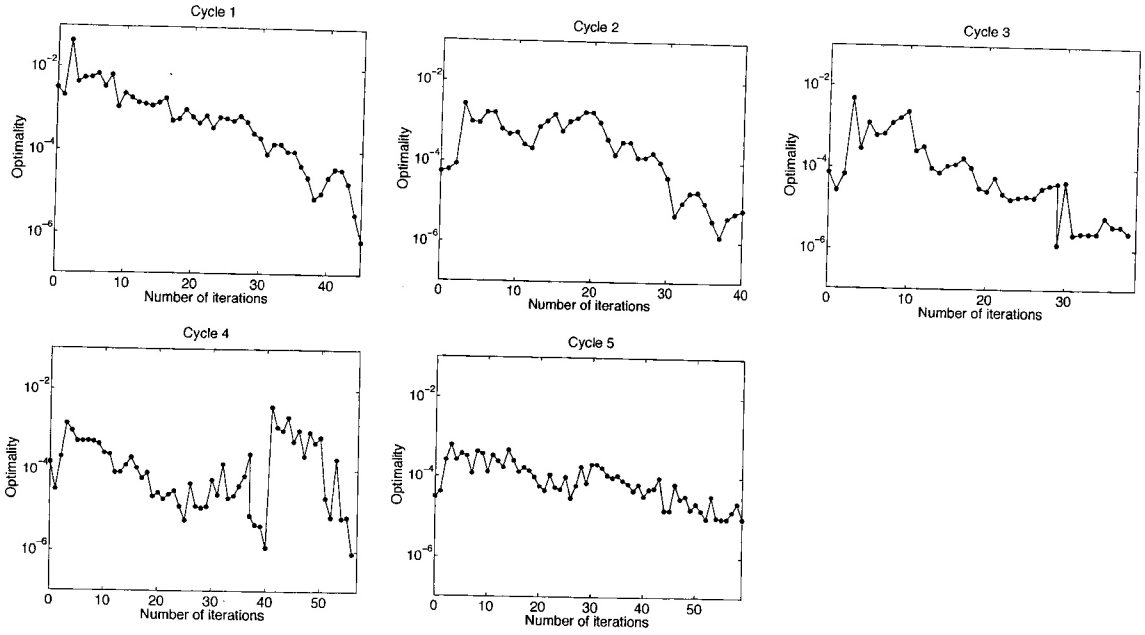

Figure A.8: Convergence History for box-wing optimization

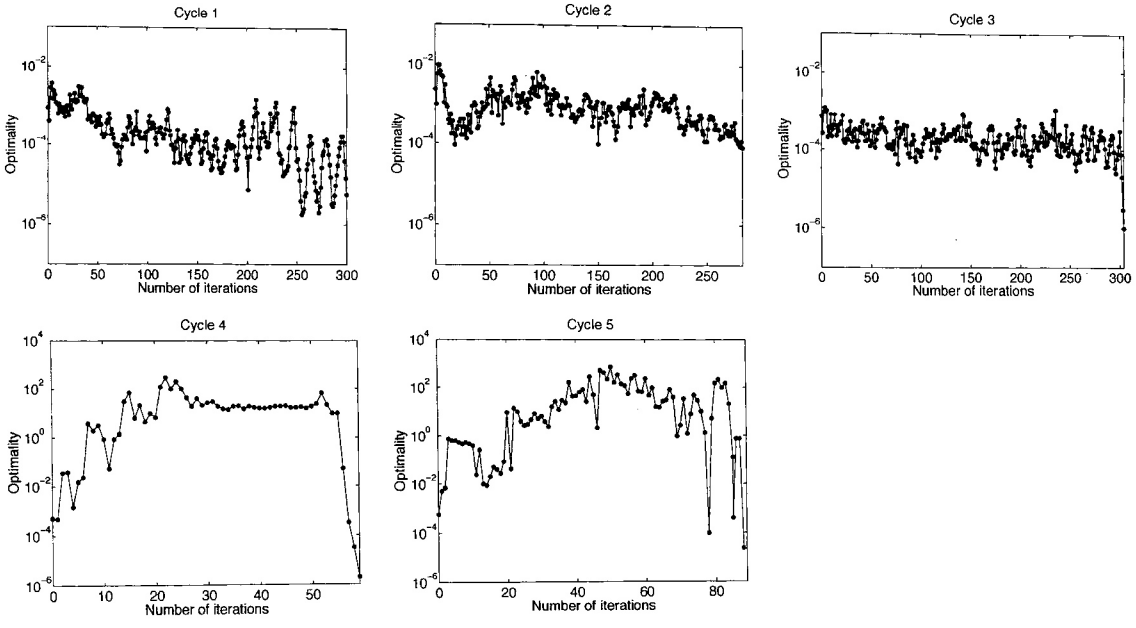

Figure A.9: Convergence History for flexible wing optimization

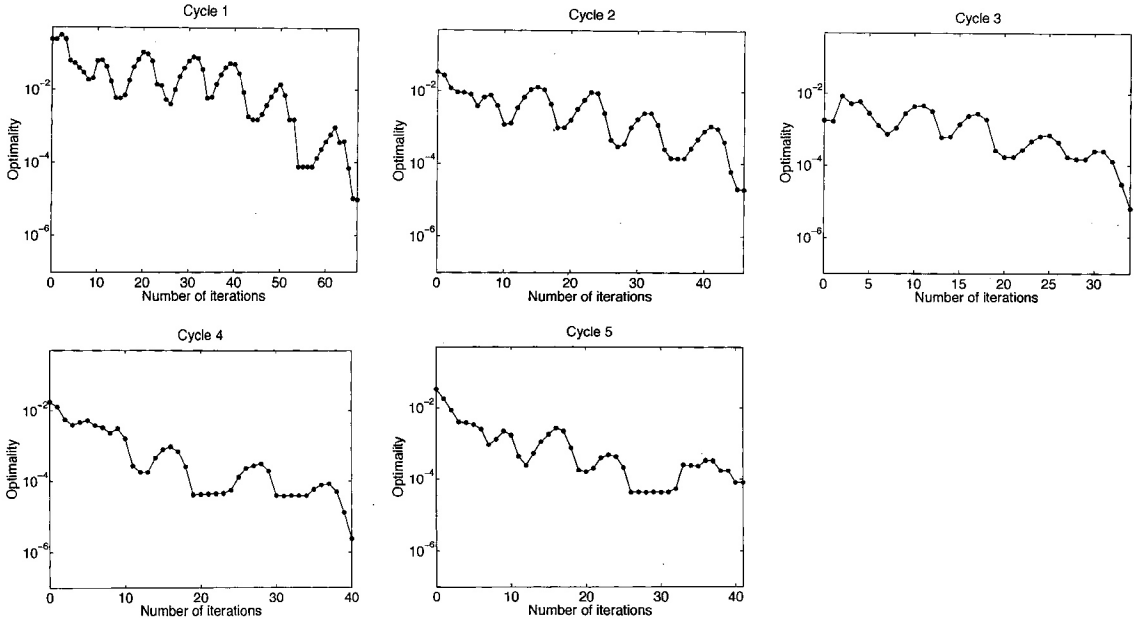

Figure A.4: Convergence History for airfoil optimizaiton case 4

A.2 Induced Drag Minimization

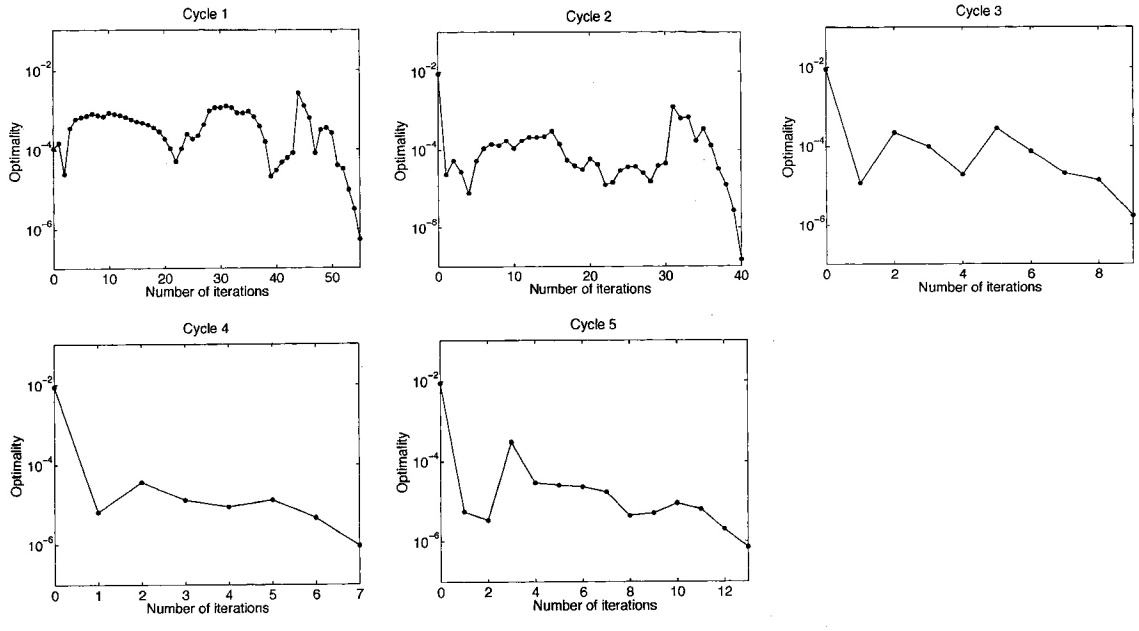

Figure A.5: Convergence History for planform optimization

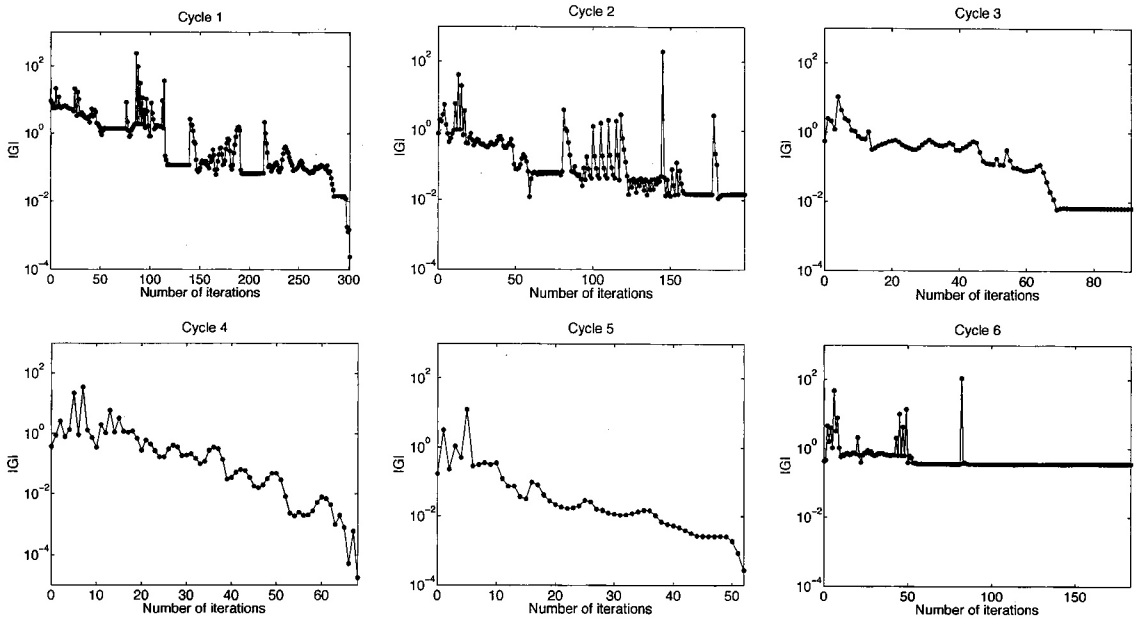

Figure A.2: Convergence history for airfoil optimization case 2

Appendix A

Convergence History

For BFGS optimizer, the convergence history are depicted in terms of the magnitude of the gradient. For SNOPT, the convergence measurement is closely related to the KKT condition. The gradient of the Lagrangian is required to be sufficient small at the convergence, thus an optimality value defined by the magnitude of this gradient and Lagrangian multipliers is used to represent the convergence history.

[34] N. Marco, J. Desideri, and S. Lanteri. Multi-objective optimization in cfd by genetic algorithms. Technical Report 3686, INRIA, 1999.

[35] M. Martinelli and F. Beux. Multi-level gradient-based methods and parametrization in aerodynamic shape design. *European Journal of Computational Mechanics*, 17(1-2):169–197, 2008.

[36] S. Mistry, H. Smith, and J. Fielding. Development of novel aircraft concepts to reduce noise and global warming effects. In *7th AIAA Aviation Technology Integration and Operations Conference*, Belfast, September 2007.

[37] B. Mohammadi. A new optimal shape design procedure for inviscid and visous turbulent flows. *International Journal for Numerical Methods in Fluids*, 25:183–203, 1997.

[38] B. Mohammadi and O. Pironneau. *Applied Shape Optimization for Fluids, Numerical Mathematics and Scientific Computation.* Oxford University press, 2001.

[39] A. Morris, C. Allen, and T. Rendall. High-fidelity aerodynamic shape optimization of modern transport wing using efficient hierarchical parameterization. *Int. J. Numer. Meth. Fluids*, 63:297–312, 2010.

[40] S. Nadarajah, P. Castonguay, and A. Mousavi. Survey of shape parameterization techniques and its effect on three dimensional aerodynamic shape optimization. In *AIAA-2007-3837, 18th AIAA Computational Fluid Dynamics Conference*, Miami, FL, 25-28 June 2007.

[41] M. Nemec and D. W. Zingg. Newton-krylov algorithm for aerodynamic design using the navier-stokes equations. *AIAA J.*, 40:1146–1154, 2002.

[42] M. Nemec, D. W. Zingg, and T. H. Pulliam. Multipoint and multi-objective aerodynamic shape optimization. *AIAA J.*, 42:1057–1065, 2004.

[43] A. Oyama, S. Obayashi, K. Nakahashi, and N. Hirose. Aerodynamic wing optimization via evolutionary algorithms based on structured coding. *Computional Fluid Dynamics Journal*, 8(4):570–577, 2000.

[44] Joyce E. Penner. *Aviation and the global atmosphere: A special report of IPCC Working Groups I and III in collab. with the Scientific Assessment Panel to the*

[10] J. Desideri, B. Abou El Majd, and A. Janka. Nested and self-adaptive Bezier parameterizations for shape optimization. In *International Conference on Control, Partial Differential Equations and Scientific Computing*, Beijing, China, 13-16 Sept 2004.

[11] R. Duvigneau. Adaptive parameterization using free-form deformation for aerodynamic shape optimization. Technical Report 5949, INRIA, 2006.

[12] R. Duvigneau, B. Chaigne, and J. Desideri. Multilevel parameterization for shape optimization in aerodynamics and electromagnetics using a particle swarm optimization algorithm. Technical Report 6003, INRIA, 2006.

[13] G. Farin. *Curves and Surfaces for Computer Aided Geometric Design - A Practical Guide*. Academic Press, Boston, 1990.

[14] R. Fletcher. *Practical Method of Optimization*. John Wiely & Sons Ltd., 2000.

[15] P. Gill, W. Murray, and M. Saunders. Snopt: An SQP algorithm for large-scale constrained optimization. *SIAM Journal on Optimization*, 12:979–1006, 2002.

[16] P. Gill, W. Murray, and M. Saunders. Users guide for sqopt version 7: Software for large-scale linear and quadratic programming. Technical report, Department of Mathematics, University of California, San Diego, La Jolla, CA, 2006.

[17] J. Hicken and D. Zingg. Integrated parametrization and grid movement using B-spline meshes. In *12th AIAA/ISSMO Multidisciplinary Analysis and Optimization Conference*, number AIAAC2008C6079, Victoria, British Columbia, Canada, 2008.

[18] J. Hicken and D. Zingg. An investigation of induced drag minimization using a parallel Newton-Krylov algorithm. In *12th AIAA/ISSMO Multidisciplinary Analysis and Optimization Conference*, number AIAA-2008-5807, Victoria, British Columbia, Canada, 2008.

[19] J. Hicken and D. Zingg. Globalization strategies for inexact-Newton solvers. In *AIAA 2009-4139, 19th AIAA Computational Fluid Dynamics*, San Antonio, Texas, 22 - 25 June 2009.

[20] J. E. Hicken and D. W. Zingg. Induced-drag minimization of nonplanar geometries based on the Euler equations. *AIAA J.*, 48(11):2564–2575, 2010.

abruptly. Therefore, further investigation is required to establish the selection criteria for ~~multiple control points~~ insertion of multiple control points.

6.1.4 Alternative parametrizations

There exists a large variety of geometry representation techniques for aerodynamic configurations. Many of them possess the flexibility to produce multiple parametrizations. Thus, the proposed optimization sequence can be naturally extended to these methods, and the unique properties associated with each parametrization method would result in different implementations and applicability for each individual case.

6.1.5 Multilevel optimization

The existing process defines the parametrization refinements as an optimization proceeds. One can also predetermine several different parametrization levels, and adopt multigrid strategies (e.g. "V" cycles) to perform an optimization among different parametrization levels.

Chapter 6

Conclusions

B-spline geometry parametrization technique is integrated with the knot insertion method providing flexible representations for aerodynamic geometries. In chapter 2, two-dimensional airfoils and three-dimensional configurations have been parametrized by planar B-spline curves and spatial B-spline volumes with finite number of control points. Adopting knot insertion method provides the capability of changing the number and the distribution of control points without modifying the shape of the existing configuration. Thus, the B-spline parametrization associated with multiple knot insertions defines an evolutionary parametrization so that an aerodynamic configuration can be represent with progressively increasing control points.

For aerodynamic shape optimizations, design variables are normally defined by geometry parametrizations. With B-spline formulations, the positions of control points are regarded as design variables. Therefore, the presence of evolutionary parametrization allows flexible design variables for a shape optimization problem. Taking advantage of this feature, a new optimization strategy is proposed. It organizes a design problem as a sequence of optimizations with the number of design variables gradually increased. The added design variables are systematically selected through sensitivity analysis and other criteria such that they significantly affect the subsequent optimal solutions, in order to achieve ideal optimal solution with a minimum number of design variables. At the end of each optimization, a series of termination criteria are employed to examine performance of the optimization sequence, and the enrichment of the parametrization occurs only if it is necessary.

The proposed optimization sequence is applied to airfoil optimization and induced drag minimization test cases in chapters 4 and 5. The optimization results display a con-

Table 5.2: Flexible wing optimization

Cycle	Number of streamwise CPs	Number of spanwise CPs	Drag coefficient
Initial	6	5	0.009412
1	6	5	0.005487
2	6	6	0.005248
3	7	6	0.005097
4	7	7	0.004739
5	8	7	0.004219

prominent. Moreover, sectional variations are also aggravated, a complex twisted shape emerges at the region close to the wing tip. Besides the effect of new control points, the planform variations are primarily due to releasing the bounds of the constraints. As can be seen from the planform shape of cycle 2 to 5, the chord lengths near the wing tip progressively increase, while the root chord continuously decreases. From cycle 2 to cycle 5, the drag coefficient is further reduced by 13.4%; this figure demonstrates that the optimization with evolutionary parametrization refinements is effective in producing efficient aerodynamic designs, and its benefit can be rather significant.

Is this demonstrated even if there is no baseline for comparison, e.g. a uniform refinement?

Can this be quantified?

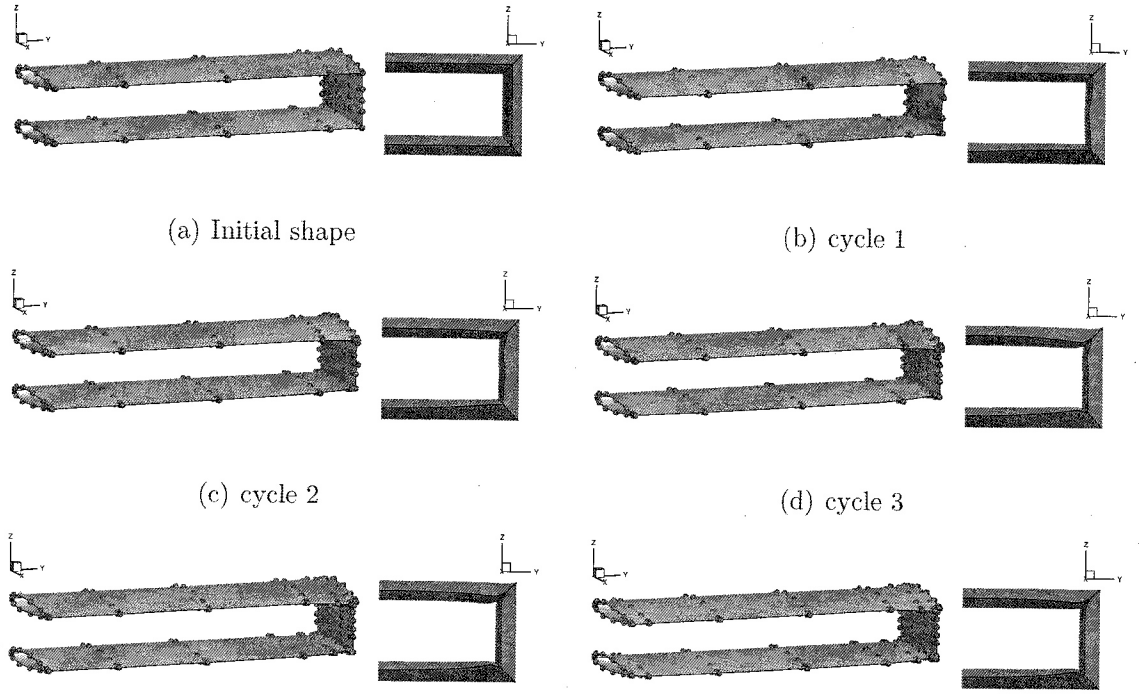

(a) Initial shape (b) cycle 1

(c) cycle 2 (d) cycle 3

(e) cycle 4 (f) cycle 5

Figure 5.7: Shape changes of the Box-wing optimization

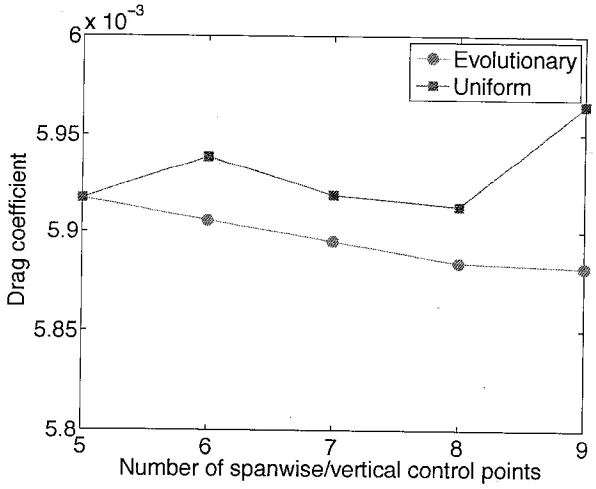

Figure 5.8: Box-wing optimization

to Case 1. The initial parametrization places 6 control points in the streamwise direction and 5 in the spanwise direction on the upper and lower surfaces of the wing. In order to reduce the possibility of multiple optima, the angle of attack is constrained to 3.939685 degrees which generates the target lift coefficient with the baseline configuration.

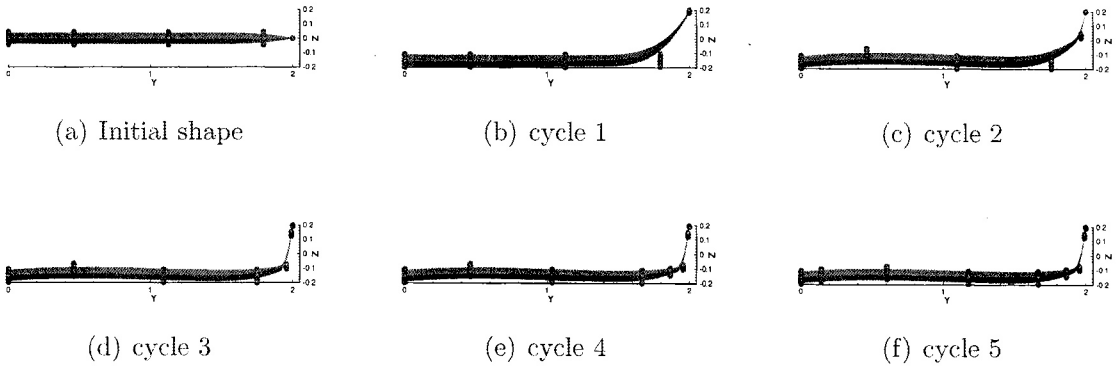

(a) Initial shape (b) cycle 1 (c) cycle 2

(d) cycle 3 (e) cycle 4 (f) cycle 5

Figure 5.5: Winglet formation

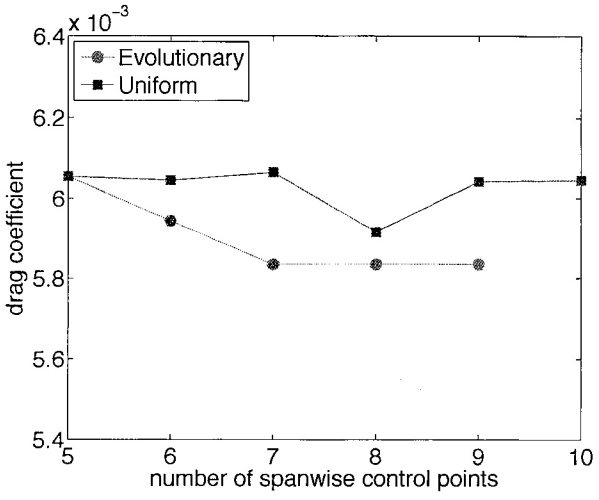

Figure 5.6: Winglet optimization

optimization sequence based on evolutionary parametrization reaches a better optimal solution with fewer design variables.

5.2.4 Case 4: Box-wing optimization

Another popular nonplanar geometry for induced drag reduction is a box-wing. In this test case, a box-wing configuration is optimized using optimization sequence with evolutionary parametrization. The baseline box-wing geometry has a semi-span of 3.0, a chord length of 1.0, and NACA0012 sections. The initial height to span ratio is 0.105. The mentioned 6-block grid is adopted, and it is initially approximated using B-spline volumes with 9 control points in the streamwise direction and 5 in the spanwise and vertical

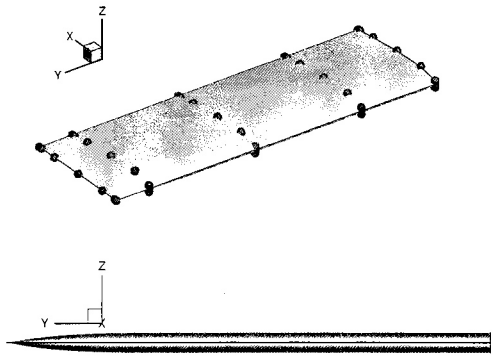

(a) Initial planform

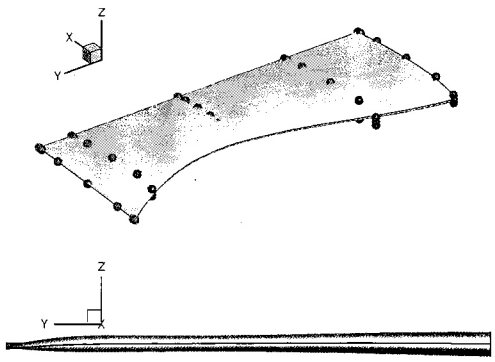

(b) cycle 1

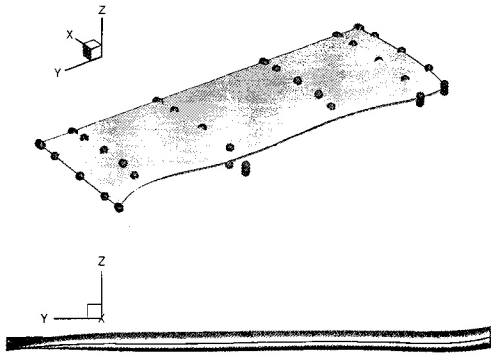

(c) cycle 2

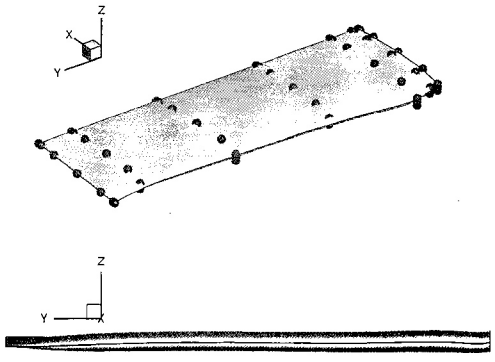

(d) cycle 3

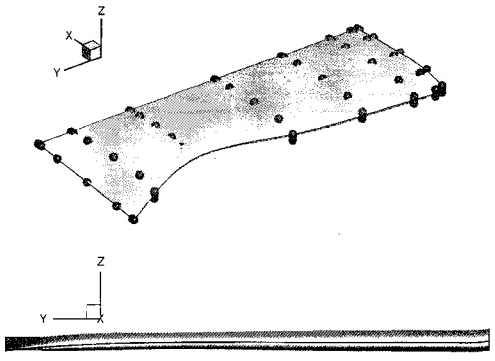

(e) cycle 4

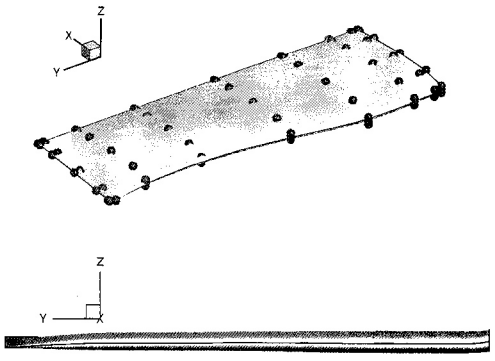

(f) cycle 5

Figure 5.3: Shape changes of the planform and twist optimization

move to next page

and a box constraint is imposed to confine the entire geometry within $-0.2 \leq z \leq 0.2$. To prevent excessive degrees of freedom, interior control points at each spanwise station are

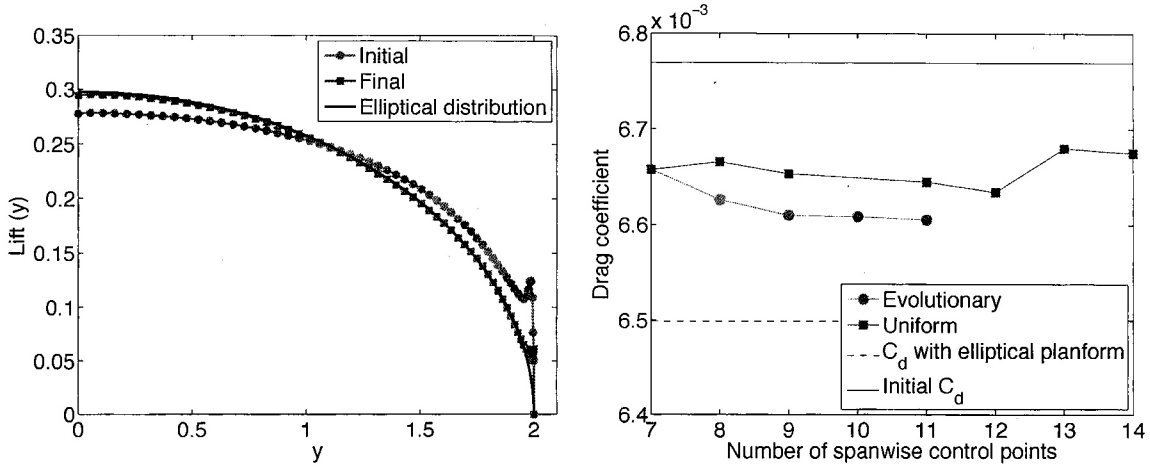

(a) Lift distribution

(b) C_D vs. number of control points

Figure 5.2: Planform optimization

5.2.2 Case 2: Planform and twist optimization

As indicated in the work by Liersch [31], an elliptical planform along does not achieve minimum induced drag, and additional twist is beneficial. The second test case is to investigate an optimal shape by varying both the planform and twist. The initial geometry is the same unswept rectangular wing used in the previous problem. The reference area, lift constraint, and the operating Mach number are also identical. The upper and lower surfaces of the wing are parametrized using 7 control points in the streamwise direction and 5 control points in the spanwise direction. The angle of attack is used as a design variable, its initial value is 3.94321 which makes the baseline geometry satisfy the lift constraint.

Different linear constraints are imposed to allow the planform and twist to vary. At each spanwise station, control points are limited to rotations and scalings defined by the leading edge and trailing edge:

$$\begin{pmatrix} x - x_{LE} \\ z - z_{LE} \end{pmatrix}_k = r_k \begin{bmatrix} \cos(\beta_k) & -\sin(\beta_k) \\ \sin(\beta_k) & \cos(\beta_k) \end{bmatrix} \begin{pmatrix} x_{TE} - x_{LE} \\ z_{TE} - z_{LE} \end{pmatrix}_k$$

Here k is the index of a spanwise station, $r_k = |x - x_{LE}|/|x_{TE} - x_{LE}|$, and $\beta_k = \arctan[(z - z_{TE})/(x - x_{TE})]$. In order to reduce the effect of a nonplanar wake, the trailing edge is fixed. Also, to prevent generating a winglet, the z coordinate of the leading edge at the wing tip is constrained to be the same as its neighbouring points, and the bending angle of two adjacent spanwsie station is restricted within 20 degrees. As a result, the

Table 5.1: Grid parameters

Grid	Blocks	Nodes	off-wall	leading edge	trailing edge	tip	off-symmetry
Flat-plate	12	1158300	0.0025	0.0025	0.0025	0.002	0.01
Box-wing	6	602258	0.002	0.002	0.002	-	0.01

5.2 Test case

5.2.1 Case 1: Planform optimization

A typical method to achieve minimum induced drag is to vary the planform shape, i.e. change chord lengths at a few spanwise stations. The flat-plate grid is approximated using B-spline volumes, and the initial geometry is constructed to be a rectangular wing with a uniform chord of 2/3, a semi-span of 2, and NACA0012 sections. The chord and span are non-dimensionlized by the chord length of the flat-plate grid. The planform area, $S = 4/3$, is used as the reference area, and remains fixed during the optimization. The freestream Mach number is 0.5, and the lift coefficient is constrained at 0.35. The initial parametrization for each block is $7 \times 7 \times 6$. In other words, on the wing surface, there are 7 control points in the streamwise and spanwise directions. The angle of attack is considered a design variable, and it is initially 3.367799 degrees, which produces the target lift coefficient with the baseline geometry.

To perform an optimization through planform variation, all the control points except the ones on the trailing edge are free to move in the streamwise direction, and the entire trailing edge is fixed to reduce the impact of a nonplanar wake. The leading edge control points possess full complete degrees of freedom; other interior points are coupled with the leading edge control points to provide a scaling once the leading edge changes. Therefore, the initial effective design variables are the 7 chord lengths and the angle of attack. One additional box constraint is imposed to confine the wing within $-0.5 \leq x \leq 0.5$. The parametrization refinement is formulated such that more spanwise stations are added. Hence, the the number of effective design variables gradually increases. By experience, each knot interval is required to maintain at least 15% of the total number of parameters in the spanwise direction, so that the B-spline control points lie sufficiently far apart.

Figure 5.1 shows the planform deformation at each optimization cycle. As the more spanwise stations are added, the geometry approaches a crescent shape with decreasing chord lengths along the span. The lift distributions are plotted in Figure 5.2(a), and it

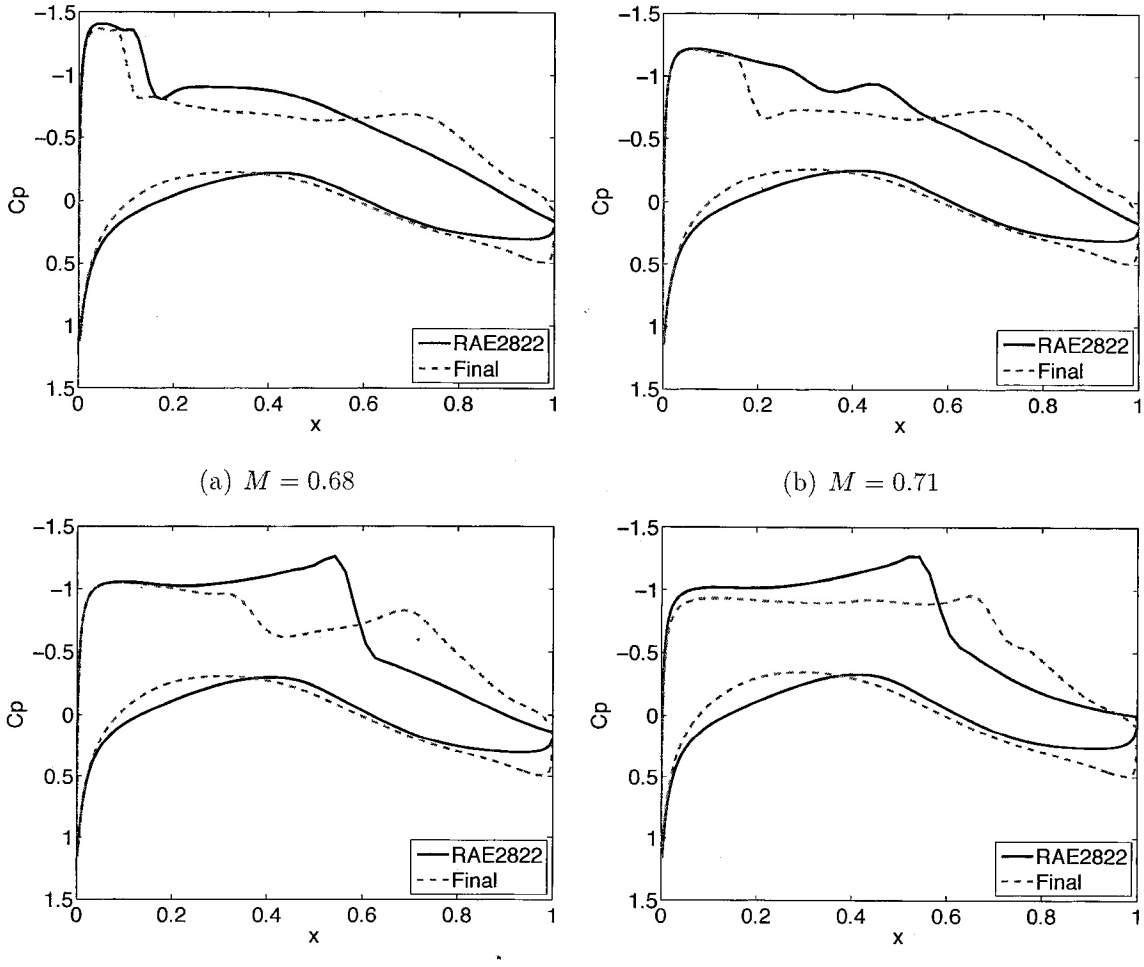

(a) $M = 0.68$ (b) $M = 0.71$

(c) $M = 0.74$ (d) $M = 0.76$

Figure 4.10: Pressure distribution for each operating point

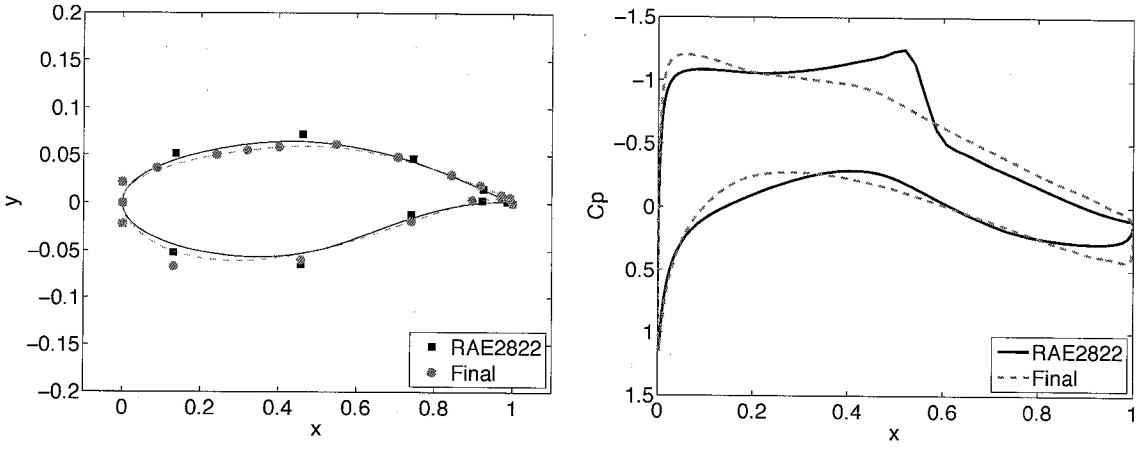

(a) Optimized geometry (b) Pressure distribution

Figure 4.7: Optimized geometry and pressure distribution of Case 3

proposed optimization sequence is able to reach an optimal solution that is comparable to the result obtained using 27 design variables evenly around the airfoil.

4.2.4 Case 4: Multipoint optimization

The last test case applies evolutionary parametrization to a multipoint optimization problem. The RAE2822 airfoil is improved over a range of Mach numbers, 0.68, 0.71, 0.74, 0.76 with associated weights of 1.0, 1.0, 2.0, 3.0. The lift coefficient is constrained at

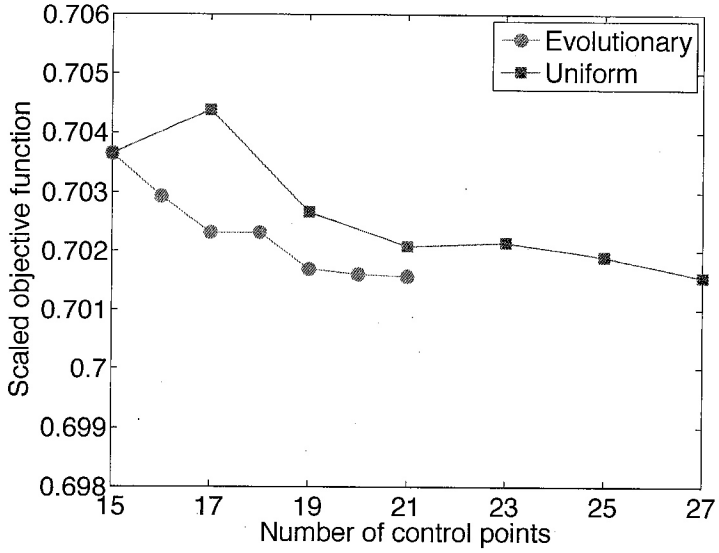

Figure 4.8: Objective function comparison of Case 3

Table 4.2: Thickness constraints for the Case 2

Thickness constraints	1	2	3	4	5	6	7
Location (c)	0.05	0.35	0.65	0.75	0.85	0.95	0.99
Thickness (c)	0.04	0.11	0.04	0.03	0.026	0.012	0.002

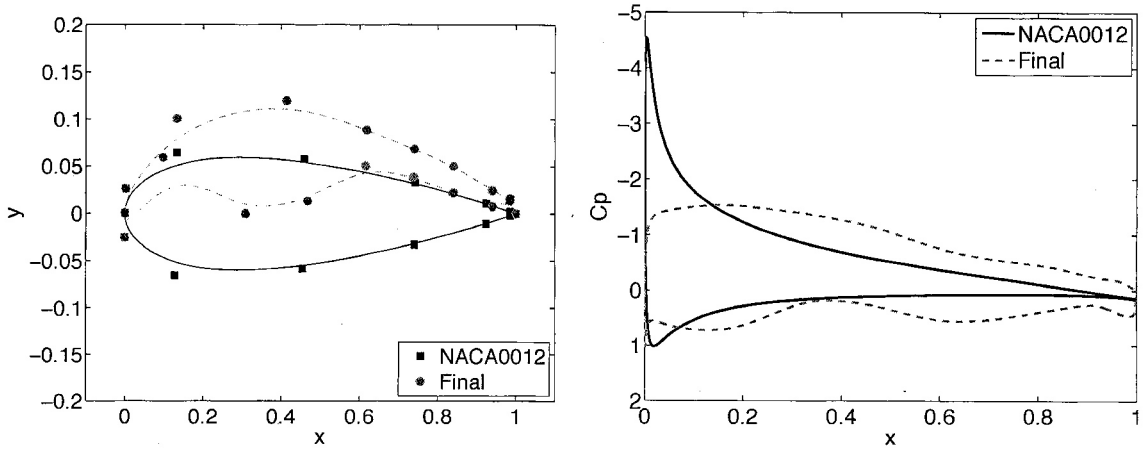

(a) Optimized geometry

(b) Pressure distribution

Figure 4.5: Optimized geometry and pressure distribution of Case 2

tions with uniform refinements are shown in Figure 4.6. The scaling factor $C_{l/d}$ is the lift-to-drag ratio of NACA0012 airfoil. The optimization with evolutionary parametrization terminates at the end of cycle 6, due to the fact that all the thickness constraints are considered. The performance of the optimization sequence confirms its efficiency of introducing essential control points. The optimal lift-to-drag ratio is obtained after adding 5 design variables. The gradient history are included in Figure A.2, and it can be seen that BFGS converges rather slower than SNOPT, so the primary optimizer used in this work is SNOPT package.

4.2.3 Case 3: Lift-constrained drag minimization (transonic)

In this test case, the drag coefficient is minimized in a transonic turbulent flow. The freestream flow has a Mach number of 0.74 and a Reynolds number of 2.7 million. The lift coefficient is constrained to be 0.733, and the geometric constraints contain area and thickness constraints (Table 4.3). The baseline shape is the RAE2822 airfoil, which is parametrized by 15 control points initially. The treatment of angle of attack is the same as Case 1.

Table 4.1: Thickness constraints for the Case 1

Thickness constraints	1	2	3	4	5	6
Location (c)	0.05	0.35	0.65	0.85	0.95	0.99
Thickness (c)	0.04	0.11	0.04	0.026	0.012	0.002

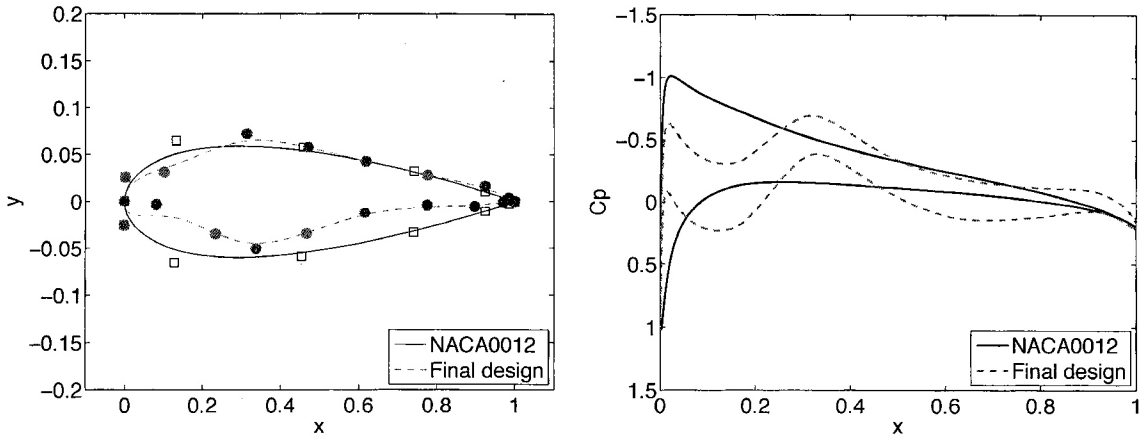

(a) Optimized geometry (b) Pressure distribution

Figure 4.3: Optimized geometry and pressure distribution of Case 1

parametrization cycles fail to provide an improvement in the objective function. Figure 4.3(a) displays the surface modification and the inserted control points upon the completion of the optimization. Figure 4.3(b) shows the comparison of the pressure distribution.

To compare the performance of the optimal solution using evolutionary parametrization with the results obtained from uniformly refined parametrizations, Figure 4.4 plots the scaled objective function values versus the number of control points. The scaling factor is the drag coefficient of NACA0012 airfoil. From this figure, a few typical features of the proposed optimization sequence can be identified. First of all, it is efficient finding critical control points. In this problem, the optimization sequence achieves a reduction of 5.96% in drag coefficient using 21 control points, but the same amount of improvement requires 33 control points if they are uniformly distributed. Secondly, in theory, there are infinitely many parametrization refinement options, but the proposed sensitivity comparisons are only carried out using finite number of candidates. It is possible that the selected refinement has a relatively large gradient among all candidates, but its absolute magnitude is still small. Therefore, it is close to a local optimum, and the im-

permitted for knot insertions.

Apart from the restriction caused by the fixed control points, the thickness constraints imposed at certain chordwise locations play a significant role in the knot insertion algorithm. Take the minimum thickness constraint displayed in Figure 4.1 as an example. This particular constraint defines the minimum distance between two surface grid points, $\mathbf{s}_1$ and $\mathbf{s}_2$. Projecting these two points on the parametric domain using Eq. 2.13, one can identify the knot intervals they reside (Figure 4.2). If the thickness constraint is active, it implies that the current design of this particular portion of the airfoil is on the edge of the design space. Thus introducing a new control point at this location has a large probability of redundancy. On the other hand, if the thickness constraint is inactive, it releases a signal that there exists a feasible region in the design space, and additional degrees of freedom may result in a better optimal solution. For the following test cases, two treatments of thickness constraints are employed:

1. If a thickness constraint is active, avoid knot insertion at the interval where the thickness constraint belongs.
2. If a thickness constraint is inactive, inserting knot at the interval where the constraint resides and its adjacent intervals is preferred. The inclusion of the neighbouring intervals is effective since kth order B-spline control points supports k knot intervals.

Finally, as mentioned in the selection criteria, to avoid accumulation of control points, the size of the knot intervals should be restricted. In the two-dimensional airfoil optimization problems, the minimum size of a knot interval is set to be 5% of the parametric domain. This number has been tested in numerous experiments, and the results indicate that it works well for airfoil optimization problems.

4.2 Test Cases

In the following test cases, the NACA0012 and RAE2822 airfoils are used as the baseline geometries for subsonic and transonic problems respectively. The adopted computational grids have a "C" topology with 289 nodes in the streamwise direction and 65 nodes in the normal direction. The normal off-wall spacing is 2×10^{-6} chord, the surface spacing at the leading edge and trailing edge are 5×10^{-4} chord and 1×10^{-3} chord, the distance to the far-field boundary is 24 chords.

2. One selection criterion uses the magnitude of the sensitivity as a test of different parametrization refinements. This is only valid if the optimization is fairly well converged.

Moreover, terminating the optimization process also requires a criterion. As pointed in the work of Zingg et al. [54], the benefit of introducing control points after a certain threshold is marginal. Thus, this process is terminated if significant improvements are not achieved by adding further design variables. Other termination conditions are also posed; they will be stated in the test cases.

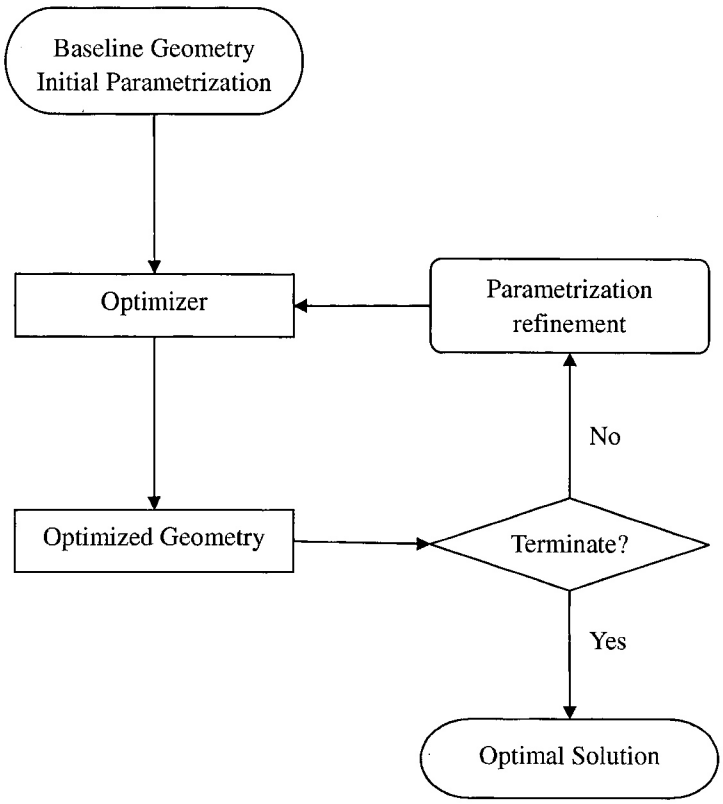

Figure 3.1: Optimization sequence with evolutionary parametrization

3.3.4 Optimization sequence

Having all the numerical routines available, an automated optimization process can be established with the aid of evolutionary B-spline parametrization. Since this evolutionary parametrization is able to produce consistent geometry representations as the number of control points gradually increases, the proposed process is executed in a progressive manner (Figure 3.1) : initially, an optimization is started with relatively few control points; once it converges or is close to convergence, the geometry parametrization is refined and the next optimization begins with more control points based on the obtained geometry. This procedure repeats continuously until the final termination. To clearly present the results, each time, finding an optimal geometry is regarded to be a completion of an optimization cycle.

Although this optimization process is carried out following a straight forward sequence, there are still some questions to be addressed during a practical implementation. First, the knot insertion algorithm can be performed at different knot intervals, so the additional control points can be placed at various locations. To choose the effec-

3.3.3 Optimization algorithm

Once an objective function and its gradient are properly defined, an optimization problem of the following form can be posed:

$$\begin{aligned} \min \quad & \mathcal{J}(\mathbf{X}) \\ \text{w.r.t} \quad & \mathbf{X} \\ \text{subject to} \quad & C_i(\mathbf{X}) \leq 0, \quad i = 1, \ldots, N_c \end{aligned}$$

where $C_i, i = 1, \ldots, N_c$ represents the imposed constraints. The presence of constraints brings significant impact on the optimization problems. Here, a summary of commonly used constraints in aerodynamic shape optimization is given.

For two-dimensional airfoil optimization:

- Lift constraint: the airfoil should maintain a specified lift coefficient during an optimization
- Thickness constraint: the airfoil thickness should exceed specified minimum thicknesses at some stations
- Range thickness constraint: the maximum thickness of an airfoil should exceed a specified value among a group of chordwise stations
- Area constraint: the enclosed area by the airfoil should exceed a specified minimum value

For three-dimensional wing optimization:

- Lift constraint: the wing should preserve a specified lift coefficient during an optimization
- Projected/surface area constraint: the wing should maintain a specified projected/wetted area
- Volume constraint: the enclosed volume by the wing should exceed a specified minimum value
- Linear constraints: some linear relations for the surface control points coupling should be stratified.

tive function. In this section, the formulations of objective function, gradient evaluation, optimization algorithm and sequence with an evolutionary parametrization are discussed.

3.3.1 Objective function

To evaluate the performance of a particular geometry, aerodynamic coefficients are usually referred to as a quantitative measure. Thus, the objective function, $\mathcal{J}$, is commonly formed by two basic coefficients, lift and drag coefficients. For instance, $\mathcal{J} = C_D$ or $\mathcal{J} = C_D/C_L$. Because the coefficients are obtained by integrating the pressure and stresses around the geometry, the objective function clearly depends on the flow solution. Moreover, the current treatment considers the angle of attack as a design variable, and the angle of attack determines the direction in which the lift and drag components are resolved. Therefore, the objective function also explicitly depends on design variables. Last, the coordinates of grid points affects the calculation of integrals, so they also appear in objective function. In general, an objective function can be represented as $\mathcal{J} = \mathcal{J}(\mathbf{Q}, \mathbf{X}, \mathbf{G})$, where $\mathbf{X}$ and $\mathbf{G}$ are design variables and grid points.

3.3.2 Gradient evaluation

To derive the proper form of the gradient, two approaches are considered. The first approach is developed by Nemec and Zingg [41], it adopts the well-known discrete adjoint method [27], and treats the sensitivity of the grid points implicitly. The final form of the gradient with respect to the design variables is given by

$$\mathcal{G} = \frac{d\mathcal{J}}{d\mathbf{X}} = \frac{\partial \mathcal{J}}{\partial \mathbf{X}} + \psi^T \frac{\partial R}{\partial \mathbf{X}} \tag{3.6}$$

$$\left[\frac{\partial R}{\partial \mathbf{Q}}\right]^T \psi = \left[\frac{\partial \mathcal{J}}{\partial \mathbf{Q}}\right]^T \tag{3.7}$$

where, $\partial \mathcal{J}/\partial \mathbf{X}$ and $\partial \mathcal{J}/\partial \mathbf{Q}$ are easy to compute either analytically or using finite differences. $\partial R/\partial \mathbf{X}$ is the term implicitly contains the sensitivity of grid points, it is also evaluated by finite differences. However, as pointed by Truong [51], if a sophisticated grid perturbation algorithm is employed, computing this partial derivative is expensive. Therefore, this approach is only used with the algebraic grid movement. Finally, $\partial R/\partial \mathbf{Q}$ is the flow Jacobian, and Eq. 3.7 is solved using the GMRES linear solver [41].

The other approach is developed by Truong et al. [51] Hicken and Zingg [18]. It extends the previous discrete adjoint approach and explicitly express the grid sensitivity

where $\begin{bmatrix}\Delta x \\ \Delta y\end{bmatrix}$ represents the shape change, and S is the normalized arclength from the airfoil surface. The normalization factor is the total arclength from the airfoil surface to the outer boundary, so the grid boundary is preserved during a perturbation.

In three-dimensional wing optimization problems, the shape change is more drastic. Hicken and Zingg [22] develop a semi-algebraic which first moves the B-spline control mesh using a incremental linear elasticity method [51], and regenerates the computational grid based on the perturbed control mesh afterwards. The linear elasticity equations are discretized using a finite element method, the resulting mesh movement residual equation is given by

$$\begin{aligned}\mathbf{r}^{(i)} &= \mathbf{r}^{(i)}(\mathbf{b}^{(i)}, \mathbf{b}^{(i-1)}) \\ &= K^{(i)}(\mathbf{b}^{(i)} - \mathbf{b}^{(i-1)}) - \mathbf{f}^{(i)}, \qquad i = 1, \ldots, m\end{aligned} \tag{3.2}$$

where $\mathbf{r}^{(i)}$ is the residual, K^i is the stiffness matrix whose elements are defined by the spatially varying Young's modulus, ~~The Young's modulus~~ is determined by the volume and distortion of each element, $\mathbf{b}^{(i)}$ are the control points vector, and $\mathbf{f}^{(i)}$ is the discrete force defined implicitly by the displacements of the surface and boundary control points. This entire procedure is done in m increments; for the optimization examples presented in this thesis, m is fixed to be 5.

3.2 Flow Solver

A high-fidelity flow solver is used to evaluate the aerodynamic performance of the existing geometry. For a two-dimensional airfoil, an efficient Newton-Krylov flow solver was developed by Nemec and Zingg [41] solving the discretized Reynolds-averaged Navier-Stokes equations with Spalart-Allmaras turbulence model. The governing equations in conservative form are given by

$$\frac{\partial \mathbf{Q}}{\partial t} + \frac{\partial \mathbf{E}}{\partial x} + \frac{\partial \mathbf{F}}{\partial y} = \frac{\partial \mathbf{E_v}}{\partial x} + \frac{\partial \mathbf{F_v}}{\partial y} \tag{3.3}$$

where $\mathbf{Q} = [\rho,\ \rho u,\ \rho v,\ e]^T$ are the conservative variables, $\mathbf{E}$ and $\mathbf{F}$ are the inviscid fluxes, $\mathbf{E_v}$ and $\mathbf{F_v}$ are the viscous fluxes. The governing equations are simplified using the thin-layer approximation and transformed to computational grid by incorporating metric terms (see the book by Pulliam and Zingg [32] for details). The second-order centred finite-difference scheme is used for spatial discretization, and the temporal derivative is

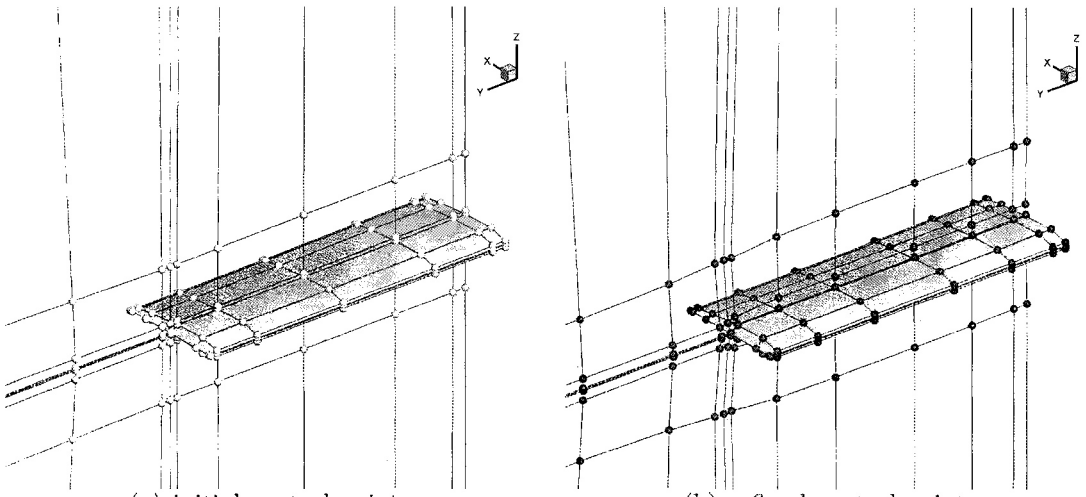

(a) initial control points (b) refined control points

Figure 2.9: Parametrization refinement of B-spline volumes. The white spheres in plot (a) are the original control points and the read spheres in plot (b) are the refined control points.

To form an evolutionary parametrization, B-spline volumes should be constructed with different numbers of control points. From Eq. 2.21, one can observe that the edge knot vectors are spatially invariant; this implies that the knot insertion algorithm for B-spline curves is still applicable to these edge knot vectors. Since the grids used in this work consist of hexahedra, once the four edge knot vectors in the same direction are refined simultaneously, all the other knot vectors in this direction can be subsequently refined using Eq. 2.21. Hence, by re-solving the least squares problem, a new B-spline volume can be established with a refined control mesh. Referring to the local support property of the B-spline formulation, only some of the control points will be altered on the edges, which implies that the change to the control mesh will be limited to the corresponding sections. Figure 2.9 illustrates a control mesh refinement of a rectangular wing in the spanwise direction (one more section is added).

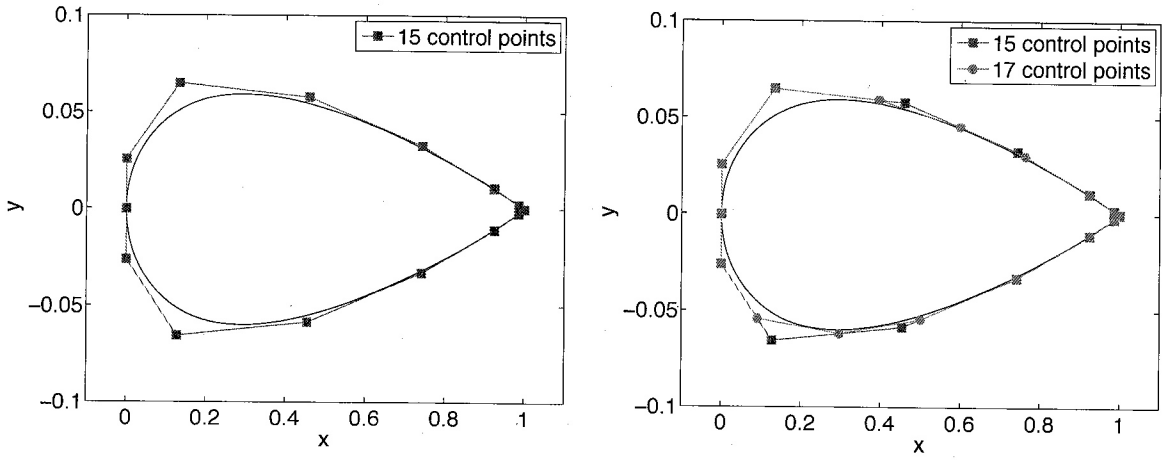

(a) initial parametrization (b) refined parametrization

Figure 2.7: B-spline parameterization of the NACA0012 airfoil. Plot (a) depicts the parametrized surface and control points; plot (b) shows the refined parametrization with the additional control points.

multi-dimensional space and it inherits all the geometric properties from B-spline curves. In the discussion of B-spline volume formulation, emphasis is given to the approximation of the computational grid and the implementation of the knot insertion algorithm.

The B-spline volume parametrization defines a mapping from a parametric space, $\{\boldsymbol{\xi} = (\xi, \eta, \zeta) \in \mathbb{R}^3 : (\xi, \eta, \zeta) \in [0, 1]\}$ to the physical space $\{\mathbf{X}(\boldsymbol{\xi}) \in \mathbb{R}^3\}$. The tensor product representation is given by

$$\mathbf{X}(\boldsymbol{\xi}) = \sum_{i=1}^{n_i} \sum_{j=1}^{n_j} \sum_{k=1}^{n_k} \mathbf{d}_{ijk}\, \mathcal{N}_{i,p_i}(\xi)\, \mathcal{N}_{j,p_j}(\eta)\, \mathcal{N}_{k,p_k}(\zeta) \tag{2.18}$$

Here, the B-spline volume $\mathbf{X}(\boldsymbol{\xi})$, and the control points, $\mathbf{d}_{ijk}$, have analogous characteristics to the B-spline curve and control points. However, the mapping parameter, $\boldsymbol{\xi}$ is defined using a traditional chord length parametrization for the purpose of approximating structured multi-block grids. The basis functions are defined separately for each parameter. Theoretically, the orders of the basis functions are independent for different parameters, but in practical applications, the order of polynomial basis functions is usually set to be the same for each parameter to maintain the same continuity condition. Hence, the order of the basis functions is denoted by p for the rest of the work. The computation of the basis functions still refers to the recursive definition but with spatially varying knot vectors. Taking basis functions in the ξ direction as an example, they are

2.2.5 B-spline curve approximation

In the context of aerodynamic shape optimization, the baseline geometry is usually not defined in B-spline formulation, but in terms of the coordinates of surface grid points. Therefore, converting this representation into B-spline form is the preliminary of an optimization. In this section, the procedure of representing a given airfoil with a 4th-order open B-spline curve is outlined.

The first essential factor is the choice of the parameter that maps the each surface point on the airfoil to the parametric domain. As denoted in the work of Kulfan [30], for an airfoil with round nose, the following centripetal parametrization [13] gives desirable results.

$$\xi_1 = 0 \tag{2.12}$$

$$\xi_j = \frac{n-k-1}{L_T}\sum_{m=1}^{j-1}\sqrt{L_m} \quad j = 2, \ldots, N \tag{2.13}$$

where N is the total number of surface points on the airfoil, L_m is the segment length between successive points, and the normalization factor, L_T is given by

$$L_T = \sum_{m=1}^{N-1}\sqrt{L_m} \tag{2.14}$$

The above mapping defines a parametric domain, $\xi \in [0, n-k-1]$. The construction of the knot vector also significantly impacts the quality of an approximation. Many authors [50, 26] have experimented with different choices. The cosine function adopted here turns out be a good compromise between robustness and accuracy:

$$t_i = \begin{cases} 0 & 1 \le i \le k \\ \frac{n-k-1}{2}\left[1 - \cos\left(\frac{i-k}{n-k-1}\pi\right)\right] & k+1 \le i \le \frac{n+k-3}{2} \\ \frac{n-k-1}{2} & \frac{n+k-1}{2} \le i \le \frac{n+k+3}{2} \\ \frac{n-k-1}{2}\left[1 - \cos\left(\frac{i-k-2}{n-k-1}\pi\right)\right] & \frac{n+k+5}{2} \le i \le n \\ n-k-1 & n+1 \le i \le n+k \end{cases} \tag{2.15}$$

Note the multiple knots appearing at the middle of the knot vector; they ensure one control point is placed at the leading edge of the airfoil. However, because the multiplicity of a knot decreases the continuity of the associated curve, the continuity reduction at the leading edge is unwanted. To overcome this problem, two adjacent control points

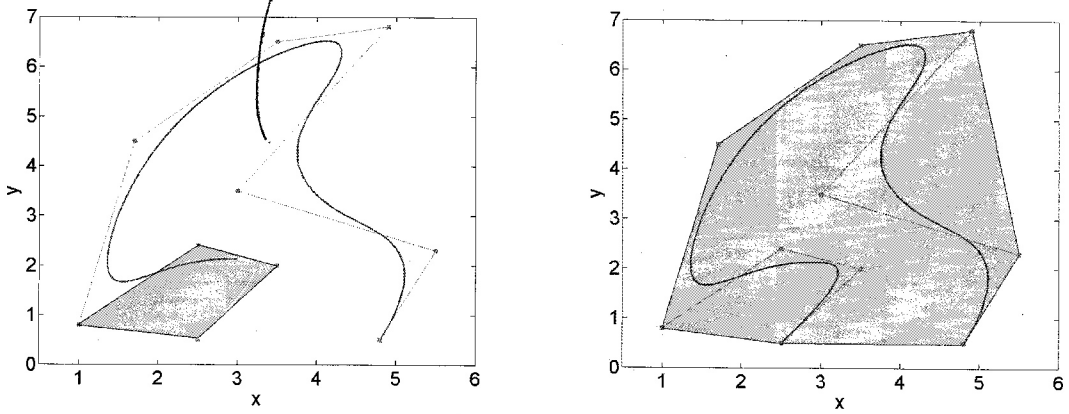

(a) Convex hull for a curve segment

(b) Convex hull for the entire curve

Figure 2.5: Convex hull property

computed as follows:

$$\frac{d}{d\xi}\mathcal{N}_{i,k} = \frac{k-1}{t_{i+k-1}-t_i}\mathcal{N}_{i,k-1} - \frac{k-1}{t_{i+k}-t_{i+1}}\mathcal{N}_{i+1,k-1} \tag{2.4}$$

Substituting these derivatives into the curve equation, the derivative of a B-spline curve is formulated by

$$\frac{d}{d\xi}\mathbf{X}(\xi) = \sum_{i=1}^{n-1}\mathcal{N}_{i+1,k-1}\frac{k-1}{t_{i+k}-t_{i+1}}(\mathbf{d_{i+1}}-\mathbf{d_i}) \tag{2.5}$$

Observing the above equation, a direct consequence can be drawn for a open B-spline curve: the derivatives of the starting and end points can written as $\frac{k-1}{t_{k+1}-t_2}(\mathbf{d_2}-\mathbf{d_1})$, $\frac{k-1}{t_{n+k-1}-t_n}(\mathbf{d_n}-\mathbf{d_{n-1}})$. Considering the fact that these two end points coincide with the first and last control points, thus the B-spline curve is tangent to $(\mathbf{d_2}-\mathbf{d_1})$ and $(\mathbf{d_n}-\mathbf{d_{n-1}})$.

2.2.4 Knot insertion

So far, a B-spline curve is defined, and its control points are normally chosen as design variables in an optimization problem to govern the shape deformation. In order to form a hierarchical parametrization suitable for multilevel optimization, a B-spline curve should be defined with flexible number of the control points, and its shape should be preserved if the number of control points changes. This requirement is accomplished through inserting an additional term in the knot vector.

Inserting a new knot obeys the following procedure. Denote the new set of control points with a superscript $*$, if a knot t^* is added to (t_r, t_{r+1}), the new control points

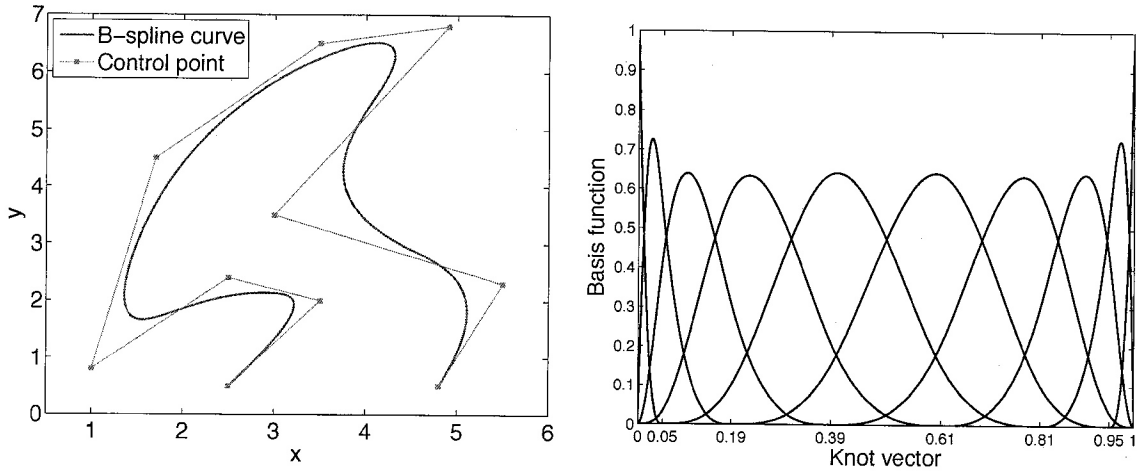

(a) B-spline curve

(b) Basis function

Figure 2.3: An open B-spline curve and its basis functions

2.2.2 B-spline control points and curves

A B-spline curve can be written as a linear combination of basis functions weighted by proper control points

$$\mathbf{X}(\xi) = \sum_{i=0}^{1} \mathbf{d}_i \mathcal{N}_{i,k}(\xi) \tag{2.3}$$

where $\mathbf{X}$ represents the B-spline curve, and the coefficient vectors, $\{\mathbf{d}_i : i = 1, \ldots, n\}$, are the coordinates of the control points. Since the parametrization in aerodynamic shape optimization extensively uses open B-spline curves, therefore, the following discussion focuses on open B-spline curves, and the boundary problem of the knot vector is resolved by placing repeated knots at both ends. Figure 2.3(a) and Figure 2.3(b) display a 4th-order open B-spline curve and its basis functions.

B-spline curves possess many favourable properties that can be used to construct a desired geometry. Some of them are direct consequence of the behaviours of the basis functions.

- An open B-spline curve passes through the two end control points $\mathbf{d}_1$ and $\mathbf{d}_n$. This is due to the fact that the two basis functions at each end of the parametric domain have the value of unity, thus Eq. 2.3 is reduced to $\mathbf{X}(\xi = 0, 1) = \mathbf{d}_i, i = 1, n$.

- Changing the position of a particular control point affects the shape of the B-spline curve locally. Since a control point is the coefficient of its corresponding basis

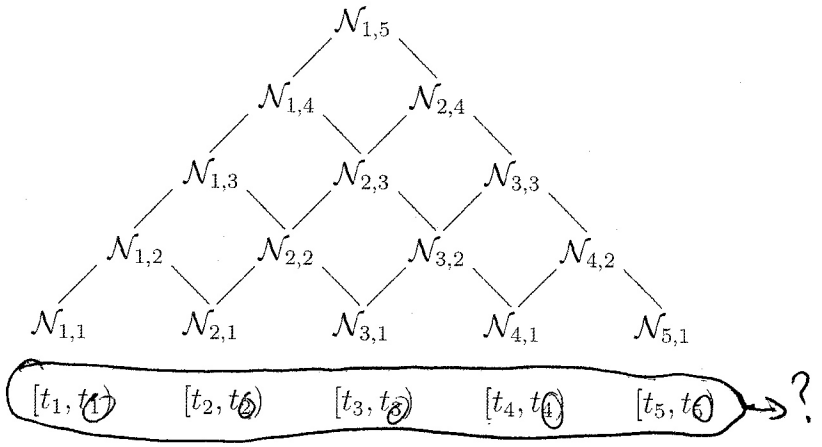

Figure 2.1: Schematic representation of the recursive relation

2.2 B-spline Curve

A planar B-spline curve, $\{\xi \in \mathbb{R} \rightarrow \mathbf{X} \in \mathbb{R}^2\}$, is the simplest geometry representation using B-spline approach, but it is effective to describe a two-dimensional object such as an airfoil. In this section, some critical B-spline properties are introduced in the context of a planar B-spline curve, but they also hold in a more general situation.

2.2.1 B-spline basis function

B-spline basis functions are polynomials of order k defined in a parametric space by the following recursive relation:

$$\mathcal{N}_{i,1}(\xi) = \begin{cases} 1 & \text{if } t_i \leq \xi \leq t_{i+1} \\ 0 & \text{otherwise} \end{cases} \tag{2.1}$$

$$\mathcal{N}_{i,k}(\xi) = \frac{\xi - t_i}{t_{i+k-1} - t_i} \mathcal{N}_{i,k-1}(\xi) + \frac{t_{i+k} - \xi}{t_{i+k} - t_{i+1}} \mathcal{N}_{i+1,k-1}(\xi) \tag{2.2}$$

The above is usually referred to as the Cox-de Boor recursion formula [8]. To visualize this recursive relation, a triangle scheme is made in Figure 2.1. From the above figure, two important observations can be concluded. First, if one traces down from a particular basis function to the lowest level, then it can be seen that a basis function, $B_{i,k}$ is non-zero at most on the interval $[t_i, t_{i+k}]$; second, if one starts with an interval, $[t_i, t_{i+1}]$, and search for the basis functions it contributes to, then it is easy to identify that at most k non-zero basis functions of order k are non-zero at this interval. The term "at most" is used because the presence of multiple knots would reduce the numbers, and these statements describe the upper limits.

parametrization for general three-dimensional objects[22]. This process consists of a B-spline approximation and a series of knot insertions. The difference of this approach and the above methods is that the knot insertion procedure is not unique due to the intrinsic properties of B-spline formulation. Therefore, parametrization refinements cannot be predetermined but can be selected during the optimization process. As a result, the proposed optimization is carried out sequentially from the initial parametrization to more refined parametrizations as long as the objective function continues to improve.

The proposed process is applied to different aerodynamic shape optimization problems, and its implementation is adjusted by considering different design problems. For airfoil optimizations, special considerations are devoted to geometric constraints; while for three-dimensional wing optimizations, different control point coupling methods are employed for different design purposes. The expected benefits of this process are mainly twofold. First, it eliminates the assumptions of the number and locations of design variables before an optimization, and prevents intervention from a designer during an optimization. Thus it may yield geometries not anticipated. Second, this process has the potential to achieve a more optimal design with fewer design variables compared to optimizations using regular parametrization strategy.

move relatively few control points, and an inexpensive algebraic method to adjust a large number of mesh points [22]. Besides these common properties, there exist unique features for individual approach. Regarding Bezier curves and surfaces, two characteristics of the basis functions limit their flexibility. First, the number of control points of a Bezier curve or surface is associated with the degree of the basis functions. In order to increase the number of control points, degree elevation of the basis functions is necessary [26, 13]. Second, a Bezier curve or surface does not provide local control. i.e. moving a control point changes the entire geometry.

The B-spline formulation [8] overcomes the mentioned disadvantages because its intrinsic basis function formulation provides local control of a parametrized shape, and its flexible knot vector structure allows additional control points to be introduced without increasing the degree of basis functions. Hence, the B-spline approach is an appropriate candidate for hierarchical parametrization. An additional advantage of the B-spline approach is that it is used in most CAD packages to represent the geometry. Therefore, it provides the most natural way to integrate the CAD geometry into the design process.

1.4 Evolutionary Parametrization

An evolutionary parametrization is indeed a sequence of parametrization refinements that gradually enlarge the set of design variables. Such a procedure relies on the characteristics of the geometry representation method. Two essential conditions are required for such a procedure:

- Multiple parametrization refinements can be carried out in a consistent manner;
- The geometry should not be changed as its parametrization is refined.

Attempts of performing optimization with a changing parametrization have been carried out by several authors. Beux and Dervieux [4] describe a gradient based multilevel optimization using surface grid point coordinates as design variables. The hierarchical parametrization is defined by extracting different subsets of grid points from the complete surface points, forming a family of embedded parametrization levels (i.e. a coarse level corresponds to a small number of grid points, and a fine level refers to a large number of points). A linear prolongation operator defined by Hermitian interpolation is used to switch between different parametrization levels. The objective function and the gradient

progressively evolve as an optimization proceeds. This type of parametrization strategy is referred to as evolutionary parametrization in this thesis. The following two sections are devoted to a brief review of existing geometry parametrization techniques and previous applications and constructions of evolutionary parametrization.

1.3 Parametrization Methods

The choice of geometry parametrization is a crucial procedure in shape optimization. A number of authors have outlined the desirable characteristics of an ideal parametrization method [47, 30, 11], and several essential criteria are worth additional emphasis:

- A parametrization should be able to provide fast, accurate and consistent representations for complex geometries
- A parametrization should produce a compact and flexible set of design variables
- A parametrization should provide easy control and interpretation for geometry deformation

A large variety of parametrization methods have been established for various applications [47, 6, 40]. An intuitive method is the discrete approach which uses surface grid point coordinates as design variables. This approach is able to describe a large number of dramatically different geometries and can also reflect subtle shape changes in a local region. However, since the shape change is tied to individual grid points, it is difficult to maintain a smooth surface profile, and there is a tendency to yield unrealistic designs, as indicated by Braibant and Fleury [5]. Another obstacle associated with this method is the excessive number of design variables. Because the stiffness of the numerical optimization increases ~~abruptly~~ greatly with the number of design variables, the efficiency of the shape optimization is adversely impacted if a fine mesh is adopted. These problems are well understood; some complementary procedures such as a smoothing routine have been established in many works [38, 37].

On the other hand, some strategies, such as extended Joukowski transformation [28] and PARSEC [43], can produce a compact set of design variables, but these methods are restricted to represent the shape of an airfoil, and lack of generality for arbitrary complex configurations. In addition, the design variables used in such a parametrization must be

1.2 Aerodynamic Shape Optimization

With the purpose of exploring novel aerodynamic configurations, the numerical shape optimization method exhibits distinct advantages comparing to the traditional "cut and try" and inverse design approaches. One significant advantage of the optimization method is that it reduces the intervention from designers. Both the "cut and try" and inverse design approaches require extensive experience from designers to either manually alter the geometry or specify the target pressure distribution, but when facing unconventional configurations or unfamiliar design objectives, the manipulation based on empirical data could mislead or restrict the design results. In contrast, the shape optimization method combines a geometry control technique and an optimization algorithm to mathematically seek optimal design. Thus an optimal configuration can be obtained through systematically and effectively searching a design space. Another prominent benefit is its capability of addressing complex design problems. Since a practical design is required to have robust performance under a range of operating conditions and constraints, the numerical shape optimization is ideal to handle the situation consisting of multiple design requirements and conditions.

A fully automated aerodynamic shape optimization contains several key components: a geometry parametrization which defines the design variables and governs shape changes; a mesh movement algorithm that perturbs the computational grid according to the geometry deformation; objective function definition that typically includes lift, drag, and moment functionals; flow analysis tool (flow solver), and optimization algorithm (optimizer). Each component influences the implementation efficiency and the optimal solution of a particular optimization process. One of the major factors is flow solver. because a flow solver is repeatedly used to obtain flow solutions for objective function evaluations, high accuracy and fast computational speed is greatly demanded. Owning to the improvement in computational fluid dynamics (CFD), and the development of computing capabilities, high fidelity analysis codes are now available to handle three-dimensional Reynolds-averaged Navier-Stocks equations within reasonable amount of time, but solving complex nonlinear flow features such as laminar-turbulence transition still remains costly tasks. Besides flow solver, optimizer also critically affects the performance of an optimization method. In most aerodynamic applications, two types of optimizers are adopted. One only makes use of the objective function value, for instance, genetic algorithms [34, 43]. This type of optimizers have a large probability of finding a global optimum, but converges

List of Tables

Contents

Abstract

An Evolutionary Geometry Parametrization for Aerodynamic Shape Optimization

Xiaocong Han
Masters of Applied Science
Graduate Department of Aerospace Engineering
University of Toronto
2011

An evolutionary geometry parametrization is established to represent aerodynamic configurations. This geometry parametrization technique is constructed by integrating the classical B-spline formulation with the knot insertion algorithm. It is capable of inserting control points to a given parametrization without modifying its geometry. Taking advantage of this technique, a shape design problem can be solved as a sequence of optimizations from the basic parametrization to more refined parametrizations. Owing to the nature of B-spline formulation, feasible parametrization refinements are not unique; guidelines based on sensitivity analysis and geometry constraints are developed to assist the automation of the proposed optimization sequence. Test cases involving airfoil optimization and induced drag minimization are solved adopting this method. Its effectiveness is demonstrated through comparisons with the optimizations using uniformly refined parametrizations.